

Whole-Molecule Approach for Determining Orientation at Isotropic Surfaces by Nonlinear Vibrational Spectroscopy

Dennis K. Hore,[†] Daniel K. Beaman,[†] Daniel H. Parks,[‡] and Geraldine L. Richmond^{*,†}

Department of Chemistry, University of Oregon, 1253 University of Oregon, Eugene, Oregon 97403, and Department of Physics, Whitman College, 345 Boyer Avenue, Walla Walla, Washington 99362

Received: May 27, 2005; In Final Form: June 13, 2005

Nonlinear vibrational spectroscopies such as visible-infrared sum-frequency spectroscopy may serve as powerful probes of interfacial structure. Obtaining quantitative orientation information, however, has been limited by the required knowledge of the corresponding molecular-level nonlinear optical properties. We provide a general scheme for calculating the vibrational hyperpolarizability of any infrared- and Raman-active mode, regardless of the molecular symmetry or complexity of the structure. Our method involves all atoms and therefore does not rely on making any local mode approximations. We show how this information is used together with experimental data to arrive at the tilt and twist angles of a surfactant headgroup at the air/water interface. Since our approach is completely general, it may be used for the analysis of any adsorbate at an isotropic interface.

1. Introduction

Surfaces and interfaces have received special attention owing to the propensity of unique chemical, physical, and biological phenomena that are manifest there. Analytical methods that are sensitive to surface properties include X-ray and neutron reflectivity, ellipsometry, Brewster angle microscopy, and attenuated total reflection infrared spectroscopy. While these techniques afford important qualitative information about the surface or buried interface under investigation, their primary deficiency in providing quantitative structural information is that they cannot distinguish the signal originating from the surface from that originating from the bulk solid or solution phase. This is because surface sensitivity in these methods relies on shallow penetration of the probe beams into the bulk phase. Vibrational sum-frequency spectroscopy^{1–7} is an ideal probe of adsorbed monolayer and interfacial structure, since, being a second-order nonlinear optical technique, it is inherently selective of non-centrosymmetric environments, and thereby excludes contributions from molecules in adjacent bulk phases. The surface specificity or “surface/bulk contrast mechanism” here comes from orientational ordering: there is no long-range order in the bulk of isotropic materials, but such macroscopic symmetry is broken at an interface.

The information provided by sum-frequency spectroscopy is highly revealing of the nature of surface species, the adsorbed surface number density, and the change of these properties with respect to any perturbations on the system, thereby revealing information about the surface dynamics. If quantitative molecular orientation information is sought, however, an obstacle presents itself. All quantitative determinations of orientation must make use of the molecular optical constants appropriate to the experiment. For example, in a simple dichroic infrared experiment, one must know the vibrational transition dipole

moment (and its orientation with respect to the nuclear framework). In the case of sum-frequency spectroscopy, it is necessary to have some measure of the hyperpolarizability, β . This is the 27-element rank-three tensor, β_{lmn} , which, when scaled by the surface number density and averaged over all participating orientations of molecules, accounts for the measured macroscopic quantity, the second-order nonlinear susceptibility, $\chi^{(2)}$.

A popular method for obtaining hyperpolarizability information based on experimental data is to make use of Raman depolarization ratios.⁸ In a polarized Raman scattering experiment, the ratio between scattered light with a polarization component parallel to the pump beam and that with a perpendicular polarization is referred to as the depolarization ratio, $\rho = I_{\perp}/I_{\parallel}$. It can be shown⁹ that this quantity is related to the ratio of polarizability tensor elements, $r = \alpha_{\perp}/\alpha_{\parallel}$. In a local mode approximation with cylindrical symmetry, one often assumes that the only non-negligible components of the polarizability tensor are along the diagonal. In that case, $\alpha_{\parallel} = \alpha_{cc}$ and $\alpha_{\perp} = \alpha_{aa} = \alpha_{bb}$. There are a few potential difficulties associated with this approach. First, the local mode may not possess cylindrical symmetry; in that case, the approximation $\alpha_{aa} = \alpha_{bb}$ and the neglect of off-diagonal elements would not be justified. Further, such a measurement requires a well-resolved Raman resonance for accurate measurement of ρ for the vibrational mode of interest. In addition, the sample must be isotropic; the smallest amount of ordering will prohibit accurate determination of r from ρ . Even when these criteria can be met, the Raman experiment often requires highly concentrated solutions which may not be representative of the molecular environment at the surface.

As an alternative to the use of depolarization ratios, a more general approach is to use the bond-additivity model,^{10–12} where the dipole moment and polarizability of a specific functional group is obtained by a linear combination of the dipole moments and polarizabilities of the individual bonds that comprise the chemical moiety. In a sum-frequency study of the neat air/water interface, Morita and Hynes¹³ used this approach to calculate

* To whom correspondence should be addressed. E-mail: richmond@uoregon.edu. Phone: 541-346-4635. Fax: 541-346-5859.

[†] University of Oregon.

[‡] Whitman College.

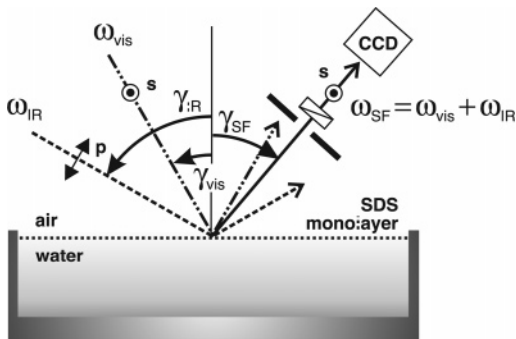


Figure 1. Side view of the sample/beam geometry, showing the visible and tunable IR beams incident at the air/solution interface. The sum-frequency beam, detected in reflection, is spatially and spectrally filtered and then detected on a two-dimensional CCD array. This also shows, as an example, the ssp polarization scheme, where the incoming visible beam is s-polarized, the IR beam is p-polarized, and the s-component of the sum-frequency passes through a polarizer in the detection arm.

dipole moment and polarizability derivatives for a single O–H stretch of water and then coupled these values to form the symmetric and antisymmetric water stretching modes. Cossee and Schachtschneider¹⁴ have provided analogous analytical solutions for the C–H stretch modes of acetone, and these formulas have been used by Yeh et. al¹⁵ for an acetone sum-frequency study. Hirose et. al¹⁰ have published similar expressions for methyl and methylene groups. The key to all of these studies is that the manner in which the individual bond stretches are coupled to produce the normal mode coordinate is known. In the general case, such symmetry analyses are not always possible. In this paper, we present a method that is fully numerical and may therefore be applied to a molecule of any symmetry (such as C_1) and of arbitrary complexity. Furthermore, the bond-additivity model is best applied to high-frequency modes such as C–H stretches;¹⁰ our method has no such constraint.

We have recently demonstrated visible-infrared sum-frequency generation of the polar headgroup of the charged alkyl surfactant sodium dodecyl sulfate (SDS) at the air/water interface.¹⁶ In that communication, we reported the results of an orientation analysis that characterized the tilt of the S–O bond connected to the alkyl chain as well as the twist angle of the S–O–C plane. In this paper, we describe the details of this whole-molecule approach used in the analysis. We will begin by providing a brief overview of the sum-frequency experiment, followed by a description of our data. We extract elements of the second-order susceptibility from the spectra and use these together with calculated elements of the hyperpolarizability tensor for the SO_3 symmetric stretch of the SDS headgroup. Our analysis of the molecular orientation then proceeds by relating these molecule- and surface-level properties in the context of an orientation distribution function which allows us to obtain values for the tilt and twist angles of the surfactant headgroup.

2. Experimental Section

In vibrational sum-frequency spectroscopy, a fixed-frequency visible beam (in this case, $\omega_{\text{vis}} = 12\,500\text{ cm}^{-1}$) and a tunable infrared beam ($\omega_{\text{IR}} = 940\text{--}1160\text{ cm}^{-1}$ here) are spatially and temporally overlapped at the sample surface. Details of our setup, including the tunable mid-IR generation, have been published previously.¹⁷ Figure 1 shows that the sum-frequency beam ($\omega_{\text{SF}} = \omega_{\text{vis}} + \omega_{\text{IR}}$) generated at the interface is collected in reflection geometry and illustrates a typical polarization

TABLE 1: Parameters Associated with the Sum-Frequency, Visible, and Infrared Beams^a

quantity	SF	visible	IR
ω/cm^{-1}	13 570	12 500	1070
γ/deg	50.9	46.3	60.0
n_{air}	1.00	1.00	1.00
n_{water}	1.33	1.33	$1.24 + 0.0427i$
L_{xx}	0.984	0.955	$1.07 - 0.00107i$
L_{yy}	0.737	0.765	$0.717 - 0.0306i$
L_{zz}	0.574	0.591	$0.598 - 0.0404i$
\hat{e}_x	$\sin \gamma_{\text{SF}}$	$\sin \gamma_{\text{vis}}$	$\sin \gamma_{\text{IR}}$
\hat{e}_y	1	1	1
\hat{e}_z	$-\cos \gamma_{\text{SF}}$	$\cos \gamma_{\text{vis}}$	$\cos \gamma_{\text{IR}}$

^a The infrared frequency is scanned from 940 to 1160 cm^{-1} , but the Fresnel factors, L_{ii} , are calculated using values of γ_{SF} and the optical constants corresponding to a SO_3 band center frequency of 1070 cm^{-1} .

scheme (selecting s- or p-polarizations for each of the three beams) used to acquire data. The intensity of the sum-frequency signal is proportional to that of the incident visible and IR beams and also to the square of the second-order nonlinear susceptibility, $\chi^{(2)}$,

$$I(\omega_{\text{SF}}) \propto |\chi_{\text{eff}}^{(2)}|^2 I(\omega_{\text{vis}}) I(\omega_{\text{IR}}) \quad (1)$$

Here, the effective second-order susceptibility, $\chi_{\text{eff}}^{(2)}$, is related to the actual second-order susceptibility by the Fresnel coefficients, L_{ii} , and unit polarization vectors, \hat{e}_i , for each beam

$$\chi_{ijk,\text{eff}}^{(2)} = (L_{ii}\hat{e}_i)_{\text{SF}} \chi_{ijk}^{(2)} (L_{jj}\hat{e}_j)_{\text{vis}} (L_{kk}\hat{e}_k)_{\text{IR}} \quad (2)$$

These quantities, including their dependence on the incident (γ_{vis} , γ_{IR}) and reflected angles (γ_{SF}), are summarized in Table 1.

Sodium dodecyl sulfate (Aldrich) was dissolved in 18.2 M Ω water (Nanopure) to make a bulk concentration of 6.2 mmol/L. Given a critical micelle concentration of 8.1 mmol/L,¹⁸ this provides near-monolayer coverage upon adsorption.

3. Results

The results of our determination of the SDS headgroup orientation at the air/water interface will be presented in three parts: (1) extraction of the macroscopic material property $\chi^{(2)}$ from the sum-frequency spectra, (2) evaluation of the microscopic molecular property β by ab initio methods, and (3) combination of these macroscopic and microscopic data to arrive at the average molecular orientation that relates these two quantities.

3.1. Obtaining Nonlinear Susceptibility Tensor Elements from the Spectra. Figure 2 shows baseline-corrected¹⁷ sum-frequency spectra of the SDS monolayer from 940 to 1160 cm^{-1} . This region displays a single sum-frequency active vibrational mode at 1070 cm^{-1} due to the headgroup SO_3 symmetric stretch.^{19–26} The spectra were fit to a line shape that accounts for homogeneous line broadening (Lorentzian profile), inhomogeneous broadening (convolution with a Gaussian profile), and the IR spectral bandwidth in

$$|\chi^{(2)}(\omega_{\text{IR}})|^2 = |\chi_{\text{NR}}^{(2)} + A \int_0^\infty \frac{1}{\omega_{\text{IR}} - \omega_L + i\Gamma_h} \exp\left[-\frac{(\omega_0 - \omega_L)^2}{2\Gamma_i^2}\right] d\omega_L|^2 \quad (3)$$

where $\chi_{\text{NR}}^{(2)}$ is the nonresonant contribution to the signal, A is the resonant amplitude, Γ_h is the homogeneous line width (fixed at 2 cm^{-1}), Γ_i is a combination of the inhomogeneous line width and IR beam spectral bandwidth (about 18 cm^{-1}), ω_0 is the

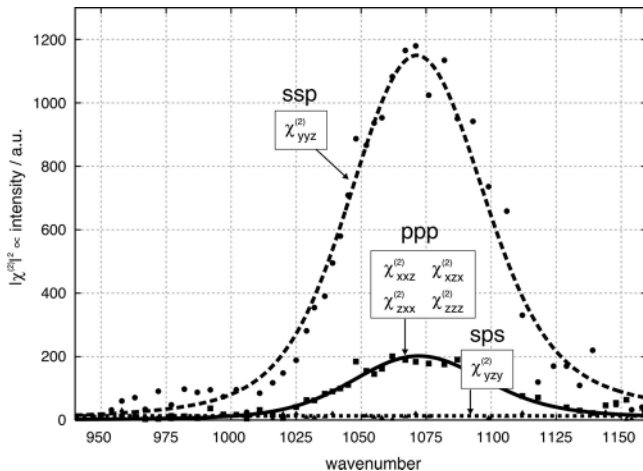


Figure 2. Results of fitting the sum-frequency data following correction of shape artifacts which result from spatial and temporal mismatch of the beams during the IR frequency scan. The spectra are labeled with the polarization scheme and the corresponding elements of the $\chi^{(2)}$ tensor which are probed.

center of the band, and ω_L is a dummy variable over which the convolution integral is evaluated. Fits to eq 3 are shown as lines in Figure 2. We have determined that $A_{\text{ssp}} = 1179 \pm 21$, $A_{\text{ppp}} = 200 \pm 40$, and $A_{\text{sps}} \approx 0$. For both ssp and ppp spectra, $\omega_0 = 1070 \pm 1 \text{ cm}^{-1}$ and Γ_h was determined to be $21.2 \pm 0.5 \text{ cm}^{-1}$.

To proceed with the orientation analysis, it is now necessary to derive the microscopic analogue of these quantities, elements of the vibrational hyperpolarizability, β .

3.2. Whole-Molecule Approach for the Calculation of Vibrational Hyperpolarizabilities. For nonresonant Raman scattering (with ω_{vis} and ω_{SF} sufficiently far from any electronic absorption band), the frequency dependence of the vibrational hyperpolarizability, β , may be expressed as

$$\beta(\omega_{\text{IR}}) = \frac{\langle g|\hat{\alpha}|\nu\rangle\langle\nu|\hat{\mu}|g\rangle}{\omega_{\text{IR}} - \omega_0 + i\Gamma_h} \quad (4)$$

where $|g\rangle$ and $|\nu\rangle$ are the vibrational ground and excited states and $\hat{\alpha}$ and $\hat{\mu}$ are the polarizability and dipole moment operators. Under the harmonic oscillator approximation, the transition matrix elements may be expressed as derivatives of the polarizability and dipole moment with respect to the normal mode coordinate, Q . Substituting

$$\langle g|\hat{\alpha}|\nu\rangle = \frac{1}{\sqrt{2m\omega_0}} \left(\frac{\partial\alpha}{\partial Q} \right) \quad \text{and} \quad \langle\nu|\hat{\mu}|g\rangle = \frac{1}{\sqrt{2m\omega_0}} \left(\frac{\partial\mu}{\partial Q} \right) \quad (5)$$

(m is the reduced mass of the SO_3 stretch) into eq 4 results in an expression for the elements of the hyperpolarizability in terms of these quantities:

$$\beta_{lmn} = \frac{1}{2m\omega_0} \left(\frac{\partial\alpha_{lm}}{\partial Q} \right) \left(\frac{\partial\mu_n}{\partial Q} \right) \frac{1}{\omega_{\text{IR}} - \omega_0 + i\Gamma_h} \quad (6)$$

To reduce the computational burden, the twelve-carbon alkyl tail of SDS was approximated by a four-carbon chain. We therefore formulate the problem of determining β values for the SO_3 symmetric stretch of SDS by calculating $\partial\alpha_{lm}/\partial Q$ and $\partial\mu_n/\partial Q$ for the SO_3 symmetric stretch for $\text{C}_4\text{H}_9\text{OSO}_3^-$ in the gas phase.

Ab initio calculations were performed using the Gaussian 03²⁷ package, at the Hartree–Fock level with the 6-311+G(d,p) basis

TABLE 2: Results of the $\partial\alpha_{lm}/\partial Q$ and $\partial\mu_n/\partial Q$ Determination from the Data Which Appear in Figure 3

Polarizability Derivatives, $\partial\alpha_{lm}/\partial Q$, in Units of \AA^2			
l, m	a	b	c
a	-6.40×10^{-1}		
b	$+4.62 \times 10^{-6}$	-5.70×10^{-1}	
c	$+3.33 \times 10^{-7}$	-1.55×10^{-2}	-6.59×10^{-1}
Dipole Moment Derivatives, $\partial\mu_n/\partial Q$, in Units of D/\AA			
a	b	c	
-1.87×10^{-6}	-5.62×10^{-1}	-2.46×10^0	

set.²⁸ After performing an initial energy minimization/geometry optimization, the molecule was rotated into the molecular frame of interest, with the c axis oriented along the O–S bond that is connected to the alkyl chain and the S–O–C bonds defining the bc plane (see Figure 5). A normal mode analysis was performed to identify the SO_3 symmetric stretch at $\sim 1070 \text{ cm}^{-1}$. This provided the transformation from Cartesian to normal mode coordinates for this mode, which was used to displace all of the atoms by their respective distances along Q to create seven geometries: one corresponding to equilibrium bond lengths, three stretched, and three compressed. The single-point energy determined for each geometry was used to ensure that the maximum stretch or compression resulted in changes in the total energy of less than one vibrational quanta. For each of these geometries, we calculated all six unique elements of the polarizability, α_{lm} (at $\omega_{\text{vis}} = 12500 \text{ cm}^{-1}$), and the three components, μ_n , of the dipole moment vector. Derivatives were evaluated by fitting the α_{lm} and μ_n values versus the normal mode coordinate, Q , to a second-order polynomial and then taking the slope at the equilibrium geometry ($Q = 0$ in Figure 3). The shapes of these curves are shown in Figure 3, and the resulting values are summarized in Table 2. Any β element may now be assembled by multiplying the appropriate $\partial\alpha/\partial Q$ and $\partial\mu/\partial Q$ elements.

3.3. Quantitative Determination of Molecular Orientation. Now that values for the hyperpolarizability elements have been obtained, the task is to relate these quantities to the measured macroscopic quantity, the second-order susceptibility, $\chi^{(2)}$. This relation may be written as

$$\chi^{(2)} = \frac{N}{\epsilon_0} \langle \beta \rangle \quad (7)$$

where N is the surface molecular number density and ϵ_0 is the vacuum permittivity. The angle brackets denote an ensemble average and therefore contain the sought orientation information.

Since the surface of a liquid has $C_{\infty v}$ symmetry, there are only 7 of the 27 elements of $\chi^{(2)}$ that are nonzero and, of these, only 4 are unique. They are $\chi_{yzy}^{(2)} = \chi_{xzx}^{(2)}$, $\chi_{yyz}^{(2)} = \chi_{xxz}^{(2)}$, $\chi_{zxy}^{(2)} = \chi_{zxx}^{(2)}$ and $\chi_{zzz}^{(2)}$. In addition to these symmetry considerations, if we also consider that the polarizability tensor is symmetric ($\alpha_{lm} = \alpha_{ml}$) in the case of nonresonant Raman scattering, this leads to $\chi_{yzy}^{(2)} = \chi_{zyy}^{(2)} = \chi_{xzx}^{(2)} = \chi_{zxx}^{(2)}$, leaving the surface with only three independent nonzero elements of $\chi^{(2)}$. We will use the notation β_{lmn} to refer to elements of β in the molecular frame where l , m , and n are any of the molecular Cartesian coordinates (a , b , or c) and the notation $\chi_{ijk}^{(2)}$ where i , j , and k are any of the lab frame Cartesian coordinates (x , y , or z). We introduce the notation

$$\beta_{ijk}(\theta, \phi, \psi) \equiv \sum_{l,m,n} U_{lmn:ijk}(\theta, \phi, \psi) \beta_{lmn} \quad (8)$$

where $U_{lmn:ijk}(\theta, \phi, \psi)$ are elements of the transformation tensor, U , which rotates the molecule's (a, b, c) coordinate system into the lab (x, y, z) coordinate system through the Euler angles θ, ϕ , and ψ . We may now express eq 7 as

$$\begin{aligned} \chi_{ijk}^{(2)} &= \frac{N}{\epsilon_0} \langle \beta_{ijk}(\theta, \phi, \psi) \rangle \\ &= \frac{N}{\epsilon_0} \frac{1}{8\pi^2} \int_0^{2\pi} \int_0^{2\pi} \int_0^\pi f(\theta, \psi) \beta_{ijk}(\theta, \phi, \psi) \sin \theta \, d\theta \, d\phi \, d\psi \end{aligned} \quad (9)$$

Since the interface between two isotropic media (such as the air/water interface) cannot support any in-plane orientation, the azimuthal angle, ϕ , is fully averaged and will not be contained in the orientation distribution function, $f(\theta, \psi)$. For simplicity (and also because the typical measurement will provide only two independent experimental ratios), we use a δ -type orientation distribution function

$$f(\theta, \psi) = \delta(\theta - \theta_0, \psi - \psi_0) \quad (10)$$

where θ_0 and ψ_0 are the average tilt and twist angles we are interested in determining. To be as general as possible (and extract the maximum orientation information), the molecule adsorbed at the surface is treated as having C_1 symmetry, so all of the 27 elements, β_{lmn} , are nonzero. Far from electronic resonance, however, the Raman tensor is symmetric, and thus, $\beta_{lmn} = \beta_{mln}$. The consequence is that only 18 of the 27 β elements are unique. We will specify the unique elements of β in lower-triangular format, as was shown for α in Figure 3 and Table 2.

The three independent nonzero elements of $\chi^{(2)}$ were probed with three polarization schemes: ssp (s-polarized sum-frequency, s-polarized visible, p-polarized IR), sps, and ppp. The ssp polarization scheme isolates $\chi_{yyz}^{(2)} = (N/\epsilon_0) \langle \beta_{yyz}(\theta, \phi, \psi) \rangle$. Substituting eqs 8 and 10 into eq 9 and performing the integration results in

$$\begin{aligned} \chi_{yyz}^{(2)} &= \frac{N}{\epsilon_0} \langle \beta_{yyz}(\theta, \phi, \psi) \rangle \\ &= \frac{N}{8\epsilon_0} \left(\cos \theta_0 [3\beta_{aac} + 3\beta_{bbc} - 2(\beta_{caa} + \beta_{cbb} - \beta_{ccc}) + \right. \\ &\quad (\beta_{aac} + \beta_{bbc} + 2(\beta_{caa} + \beta_{cbb} - \beta_{ccc})) \cos 2\theta_0 + \\ &\quad 2((-\beta_{aac} + \beta_{bbc} - 2\beta_{caa} + 2\beta_{cbb}) \cos 2\psi_0 + \\ &\quad 2(\beta_{bac} + \beta_{cab} + \beta_{cba}) \sin 2\psi_0) \sin^2 \theta_0] + \\ &\quad \frac{1}{2} \sin \theta_0 [\cos \psi_0 (-5\beta_{aaa} + 2\beta_{bab} - 7\beta_{bba} + \\ &\quad 8\beta_{cac} - 4\beta_{cca} - (3\beta_{aaa} + 2\beta_{bab} - 8\beta_{cac} - \\ &\quad 4\beta_{cca}) \cos 2\theta_0) + (7\beta_{aab} - 2\beta_{baa} + 5\beta_{bbb} - 8\beta_{cbc} + \\ &\quad 4\beta_{ccb} + (\beta_{aab} + 2\beta_{baa} + 3\beta_{bbb} - 8\beta_{cbc} - \\ &\quad 4\beta_{ccb}) \cos 2\theta_0) \sin \psi_0 - 2((-\beta_{aaa} + 2\beta_{bab} + \\ &\quad \beta_{bba}) \cos 3\psi_0 + (\beta_{aab} + 2\beta_{baa} - \\ &\quad \beta_{bbb}) \sin 3\psi_0) \sin^2 \theta_0] \left. \right) \sin \theta_0 \end{aligned} \quad (11)$$

Similarly, the sps polarization scheme probes

$$\begin{aligned} \chi_{yzy}^{(2)} &= \frac{N}{\epsilon_0} \langle \beta_{yzy}(\theta, \phi, \psi) \rangle \\ &= \frac{N}{16\epsilon_0} \left([(\beta_{aac} + \beta_{bbc} + 2(\beta_{caa} + \beta_{cbb} - \beta_{ccc})) \cos 3\theta_0 + \right. \\ &\quad \cos \theta_0 (-\beta_{aac} - \beta_{bbc} + 6(\beta_{caa} + \beta_{cbb}) + 2\beta_{ccc} + \\ &\quad 4((-\beta_{aac} + \beta_{bbc} - 2\beta_{caa} + 2\beta_{cbb}) \cos 2\psi_0 + \\ &\quad 2(\beta_{bac} + \beta_{cab} + \beta_{cba}) \sin 2\psi_0) \sin^2 \theta_0] + \\ &\quad \sin \theta_0 [\cos \psi_0 (-5\beta_{aaa} - 6\beta_{bab} + \beta_{bba} + 4\beta_{cca} - \\ &\quad (3\beta_{aaa} + 2\beta_{bab} + \beta_{bba} - 8\beta_{cac} - 4\beta_{cca}) \cos 2\theta_0) + \\ &\quad (-\beta_{aab} + 6\beta_{bba} + 5\beta_{bbb} - 4\beta_{ccb} + (\beta_{aab} + 2\beta_{baa} + \\ &\quad 3\beta_{bbb} - 8\beta_{cbc} - 4\beta_{ccb}) \cos 2\theta_0) \sin \psi_0 - 2((-\beta_{aaa} + \\ &\quad 2\beta_{bab} + \beta_{bba}) \cos 3\psi_0 + (\beta_{aab} + 2\beta_{baa} - \\ &\quad \beta_{bbb}) \sin 3\psi_0) \sin^2 \theta_0] \left. \right) \sin \theta_0 \end{aligned} \quad (12)$$

The ppp polarization scheme probes four elements of the second-order susceptibility: $\chi_{xxz}^{(2)}$ (identical to $\chi_{yyz}^{(2)}$), $\chi_{zxx}^{(2)}$ and $\chi_{zzx}^{(2)}$ (both identical to $\chi_{yzy}^{(2)}$), and one additional element

$$\begin{aligned} \chi_{zzz}^{(2)} &= \frac{N}{\epsilon_0} \langle \beta_{zzz}(\theta, \phi, \psi) \rangle \\ &= \frac{N}{8\epsilon_0} \left([2 \cos \theta_0 (\beta_{aac} + \beta_{bbc} + 2(\beta_{caa} + \beta_{cbb} + \beta_{ccc}) - \right. \\ &\quad (\beta_{aac} + \beta_{bbc} + 2(\beta_{caa} + \beta_{cbb} - \beta_{ccc})) \cos 2\theta_0 - \\ &\quad 2((-\beta_{aac} + \beta_{bbc} - 2\beta_{caa} + 2\beta_{cbb}) \cos 2\psi_0 + \\ &\quad 2(\beta_{bac} + \beta_{cab} + \beta_{cba}) \sin 2\psi_0) \sin^2 \theta_0] + \\ &\quad [\sin \theta_0 (-3\beta_{aaa} + 2\beta_{bab} + \beta_{bba} + 8\beta_{cac} + \\ &\quad 4\beta_{cca}) \cos \psi_0 + (3\beta_{aaa} + 2\beta_{bab} + \beta_{bba} - \\ &\quad 8\beta_{cac} - 4\beta_{cca}) \cos \psi_0 \cos 2\theta_0 + (\beta_{aab} + 2\beta_{baa} + \\ &\quad 3\beta_{bbb} + 8\beta_{cbc} + 4\beta_{ccb} - (\beta_{aab} + 2\beta_{baa} + 3\beta_{bbb} - \\ &\quad 8\beta_{cbc} - 4\beta_{ccb}) \cos 2\theta_0) \sin \psi_0 + 2((-\beta_{aaa} + \\ &\quad 2\beta_{bab} + \beta_{bba}) \cos 3\psi_0 + (\beta_{aab} + 2\beta_{baa} - \\ &\quad \beta_{bbb}) \sin 3\psi_0) \sin^2 \theta_0] \left. \right) \sin \theta_0 \end{aligned} \quad (13)$$

It is important to emphasize that eqs 11–13 are generally applicable to any isotropic interface, whether the description is for an adsorbate or molecules of the neat interface. These expressions contain all elements of β for the case of arbitrary (C_1) symmetry. (For molecules with higher symmetry, some of the β elements will be equivalent and others will be equal to zero, simplifying eqs 11–13.) By taking ratios of effective second-order susceptibilities (making use of eq 2),

$$\frac{\chi_{sps,eff}^{(2)}}{\chi_{ssp,eff}^{(2)}} = \frac{\chi_{yyz,eff}^{(2)}}{\chi_{yzy,eff}^{(2)}} \bigg|_{(\beta_{lmn}; \theta, \psi)} = \frac{A_{sps}}{A_{ssp}} \bigg|_{\text{expt}} \quad (14)$$

and

$$\begin{aligned} \chi_{ppp,eff}^{(2)} &= \\ \chi_{ssp,eff}^{(2)} &= \frac{\chi_{xxz,eff}^{(2)} + \chi_{zxx,eff}^{(2)} + \chi_{zzx,eff}^{(2)} + \chi_{zzz,eff}^{(2)}}{\chi_{yzy,eff}^{(2)}} \bigg|_{(\beta_{lmn}; \theta, \psi)} = \frac{A_{ppp}}{A_{ssp}} \bigg|_{\text{expt}} \end{aligned} \quad (15)$$

These ratios eliminate the dependence on the surface number

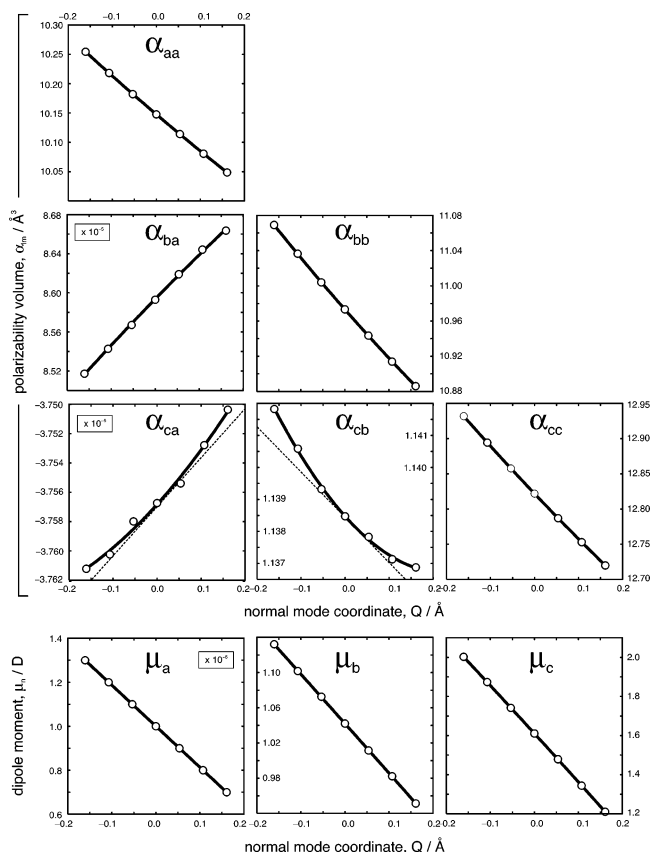


Figure 3. In the ab initio calculations, the atoms were displaced along the normal mode coordinate, Q , to create seven input geometries centered about the equilibrium geometry. For each of these structures, values of the polarizability tensor, α_{lm} (at $\omega_{\text{vis}} = 12\,500\text{ cm}^{-1}$), and dipole moment vector, μ_n , were calculated (white circles). To evaluate the derivatives with respect to Q , the data were fit to a second-order polynomial (solid lines), and the tangent at the equilibrium geometry was determined (dashed lines). Results are shown in Table 2.

density, N . In addition, the prefactor $(2m\omega_0)^{-1}$ and the Lorentzian denominator in eq 6 will cancel, allowing the product $(\partial\alpha_{lm}/\partial Q)(\partial\mu_n/\partial Q)$ to be used directly in place of β_{lmn} . (If, instead of taking ratios, eq 7 is to be used directly, experimental $\chi^{(2)}$ values need to be determined to absolute scale. We have previously described a procedure for this.²⁹)

Figure 4 shows a map of the fitting (the sum of the squares of the residuals), assuming a δ -type distribution for θ and ψ , using an explicit form of eqs 14 and 15 obtained by substituting expressions for $\chi^{(2)}$ that contain the 18 unique elements of β . Lower contours indicate a better fit between $\chi^{(2)}$ and $\langle\beta\rangle$. Values of θ greater than 25° are not shown, since the fitting error is so large in that region that detail would be lost around the displayed global minimum. The azimuthal angle, ϕ , was assumed to be uniformly distributed between 0 and 360° on account of the macroscopic $C_{\infty v}$ symmetry at the air/water interface. The substantially greater depth of the minimum at $\psi_0 = 270^\circ$ compared to the fit value at $\psi_0 = 90^\circ$ supports our determination of the S–O–C plane orientation. We have determined $\theta_0 = 16.5 \pm 9^\circ$ and $\psi_0 = 270 \pm 2^\circ$; this geometry is depicted in Figure 5.

4. Discussion

The SO_4 headgroup of SDS provides an excellent demonstration of the capability of this whole-molecule approach for determining the required vibrational hyperpolarizabilities over other methods. For SDS, it is not possible to obtain the depolarization ratio from Raman spectra, since the SO_3 sym-

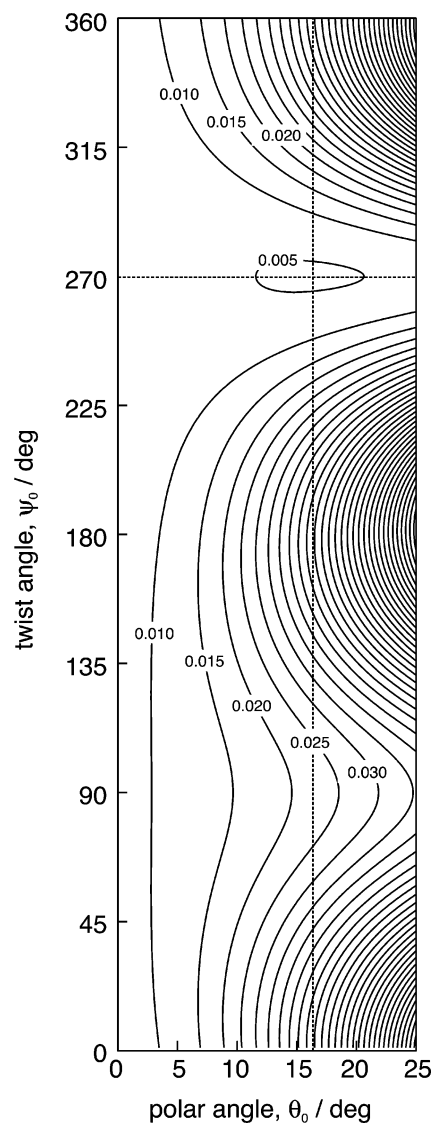


Figure 4. The calculated hyperpolarizability tensor (molecular frame) was compared to the measured second-order susceptibility tensor (lab frame) in the context of a δ -type distribution for the polar angle, θ , and the twist angle, ψ . The azimuthal angle, ϕ , was assumed to be uniformly distributed between 0 and 360° on account of the $C_{\infty v}$ symmetry at the air/water interface. From this, we have determined $\theta_0 = 16.5 \pm 9^\circ$ and $\psi_0 = 270 \pm 2^\circ$. The fitting map shows that the minimum at $\psi_0 = 270^\circ$ is considerably deeper than for the conformation where the S–O–C plane would be twisted at $\psi_0 = 90^\circ$.

metric stretch is coincident with a chain C–C mode at 1070 cm^{-1} .²⁵ In addition, there would be a further consequence in the use of ρ to approximate β , which results from the accompanying assumption of cylindrical ($C_{\infty v}$) symmetry. In fact, even if the bond-additivity model were applied, making use of the pseudo- C_{3v} symmetry of the SO_3 mode, such a detailed description of the headgroup orientation would not be possible. This is because there would be only one Euler angle, θ , that would describe the inclination of the local pseudo- C_3 axis with the surface normal, \hat{z} . If C_{3v} were in fact a good approximation for the geometry of this local mode, then that should be the maximum information obtainable from our experiment. However, our normal mode analysis has shown that there is a significant amount of wagging of the S–O bond attached to the alkyl chain during the stretching of the three terminal S–O bonds. In this case, considering the motions of all the atoms to numerically construct the normal mode coordinate allows for the determination of the orientation of

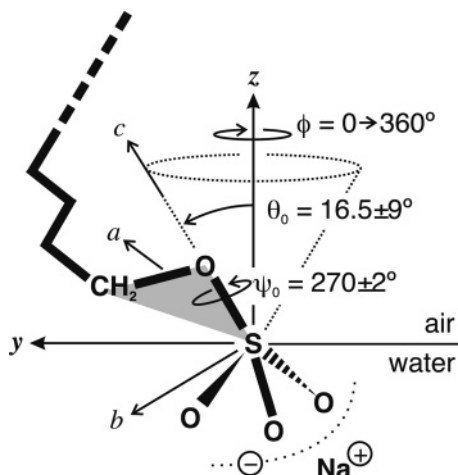


Figure 5. SDS headgroup at the air/water interface, showing the tilt and twist of the S–O–C plane. The effect of a twist specified by $\psi = 270^\circ$ is that the oxygen of the S–O–C plane always points up toward the air. In contrast, $\psi = 90^\circ$ would orient the S–O–C plane such that its oxygen would point down toward the water for any azimuth, ϕ .

the S–O–C plane (specified by θ and ψ) rather than being limited to the z –S–O angle (θ). Consequently, our analysis is able to provide a more feature-rich description of the molecular orientation than would be obtained by making a higher-symmetry local mode approximation.

We now discuss the implications of our results for the SDS monolayer structure.¹⁶ This orientation of the S–O–C plane (illustrated in Figure 5) indicates that the alkyl chain is initially oriented along the air/water interface. This initial orientation does not likely persist to the end of the chain given that other studies³⁰ have shown that the terminal methyl groups are oriented perpendicular to the water surface. In addition, various vibrational spectroscopies^{18,24,31–33} have concluded that SDS at near-monolayer concentration contains a large number of gauche defects and propose that the chains are therefore not well-ordered. Our analysis suggests a *systematic* gauche defect near the headgroup which turns the chain up so it tends perpendicular to the air/water interface. This would provide a monolayer height consistent with that reported by neutron scattering studies³⁴ and an effective headgroup area consistent with that reported by surface tension measurements.^{18,34} These results provide an experimental verification of the surfactant structure calculated by Dominguez and Berkowitz in their molecular dynamics simulations.³⁵ Our insight into this structure would not have been possible if we made a local C_{3v} approximation and then used either bond-additivity or Raman depolarization methods for obtaining the necessary vibrational hyperpolarizability elements.

5. Conclusions

This paper has demonstrated a whole-molecule approach for calculating all necessary elements of the hyperpolarizability for any vibrational mode of interest. It has been shown that these β elements may be used to determine the molecular orientation of any molecule from measured elements of the nonlinear susceptibility tensor. This information has been used to characterize the SDS headgroup at an air/water interface. Our approach for obtaining the molecular-level optical constants allows for a level of structural detail to be elucidated beyond what would have been obtainable using other methods which make approximations about the local symmetry of the functional group. Our approach is generally applicable to the analysis of any adsorbate at a vapor/liquid or liquid/liquid interface.

Acknowledgment. We wish to thank J. Hardwick for helpful discussions concerning the ab initio calculations and M. Kido for valuable insight in the orientation analysis. We thank the National Science Foundation (grant CHE-0243856) for support of this science and the Office of Naval Research for the instrumentation.

References and Notes

- (1) Shen, Y. R. Surface Spectroscopy by Nonlinear Optics. In *Proceedings of the International School of Physics "Ernesto Fermi"*; Hansch, T. W., Inguscio, M., Eds.; North-Holland: Amsterdam, The Netherlands, 1994.
- (2) Shen, Y. R. *The Principles of Nonlinear Optics*; John Wiley & Sons: New York, 1984.
- (3) Shen, Y. R. *Annu. Rev. Phys. Chem.* **1989**, *40*, 327.
- (4) Richmond, G. L. *Chem. Rev.* **2002**, *102*, 2693.
- (5) Richmond, G. L. *Annu. Rev. Phys. Chem.* **2001**, *52*, 357.
- (6) Eisenthal, K. B. *Chem. Rev.* **1996**, *96*, 1343.
- (7) Williams, C. T.; Beattie, D. A. *Surf. Sci.* **2002**, *500*, 545.
- (8) Tyrode, E.; Johnson, C. M.; Baldelli, S.; Leygraf, C.; Rutland, M. W. *J. Phys. Chem. B* **2005**, *109*, 329.
- (9) Ferraro, J. R.; Nakamoto, Z.; Brown, C. W. *Introductory Raman Spectroscopy*; Academic Press: San Diego, CA, 2003.
- (10) Hirose, C.; Akamatsu, N.; Domen, K. *J. Chem. Phys.* **1992**, *96*, 997.
- (11) Ji, N.; Shen, Y.-R. *J. Chem. Phys.* **2004**, *120*, 7107.
- (12) Lu, R.; Gan, W.; Wu, B.; Chen, H.; Wang, H. *J. Phys. Chem. B* **2004**, *108*, 7297.
- (13) Morita, A.; Hynes, J. T. *Chem. Phys.* **2000**, *258*, 371.
- (14) Cossee, P.; Schachtschneider, J. H. *J. Chem. Phys.* **1966**, *44*, 97.
- (15) Yeh, Y. L.; Zhang, C.; Heid, H.; Mebel, A. M.; Wei, X.; Lin, S. H.; Shen, Y. R. *J. Chem. Phys.* **2001**, *114*, 1837.
- (16) Hore, D. K.; Beaman, D. K.; Richmond, G. L. *J. Am. Chem. Soc.* **2005**, *127*, 9356.
- (17) Hore, D. K.; King, J. L.; Moore, F. G.; Alavi, D. S.; Hamamoto, M. Y.; Richmond, G. L. *Appl. Spectrosc.* **2004**, *58*, 1377.
- (18) Kawai, T.; Kamio, H.; Kondo, T.; Kon-No, K. *J. Phys. Chem. B* **2005**, *109*, 4497.
- (19) Li, H.; Tripp, C. P. *J. Phys. Chem. B* **2004**, *108*, 18318.
- (20) Picquart, M. *J. Phys. Chem.* **1986**, *90*, 243.
- (21) Kawai, T.; Umemura, J.; Takenaka, T. *Bull. Inst. Chem. Res., Kyoto Univ.* **1983**, *61*, 314.
- (22) Sperline, R. P.; Song, Y.; Freiser, H. *Langmuir* **1992**, *8*, 2183.
- (23) Chihara, G. *Chem. Pharm. Bull.* **1960**, *8*, 988.
- (24) Prosser, A. J.; Franses, E. J. *Langmuir* **2002**, *18*, 9234.
- (25) Brooker, M. H. *J. Chem. Soc., Faraday Trans. 1* **1984**, *80*, 73.
- (26) Thompson, W. K. *Spectrochim. Acta* **1974**, *30A*, 117.
- (27) Frisch, M. J.; Trucks, G. W.; Schlegel, H. B.; Scuseria, G. E.; Robb, M. A.; Cheeseman, J. R.; Montgomery, J. A., Jr.; Vreven, T.; Kudin, K. N.; Burant, J. C.; Millam, J. M.; Iyengar, S. S.; Tomasi, J.; Barone, V.; Mennucci, B.; Cossi, M.; Scalmani, G.; Rega, N.; Petersson, G. A.; Nakatsuji, H.; Hada, M.; Ehara, M.; Toyota, K.; Fukuda, R.; Hasegawa, J.; Ishida, M.; Nakajima, T.; Honda, Y.; Kitao, O.; Nakai, H.; Klene, M.; Li, X.; Knox, J. E.; Hratchian, H. P.; Cross, J. B.; Bakken, V.; Adamo, C.; Jaramillo, J.; Gomperts, R.; Stratmann, R. E.; Yazyev, O.; Austin, A. J.; Cammi, R.; Pomelli, C.; Ochterski, J. W.; Ayala, P. Y.; Morokuma, K.; Voth, G. A.; Salvador, P.; Dannenberg, J. J.; Zakrzewski, V. G.; Dapprich, S.; Daniels, A. D.; Strain, M. C.; Farkas, O.; Malick, D. K.; Rabuck, A. D.; Raghavachari, K.; Foresman, J. B.; Ortiz, J. V.; Cui, Q.; Baboul, A. G.; Clifford, S.; Cioslowski, J.; Stefanov, B. B.; Liu, G.; Liashenko, A.; Piskorz, P.; Komaromi, I.; Martin, R. L.; Fox, D. J.; Keith, T.; Al-Laham, M. A.; Peng, C. Y.; Nanayakkara, A.; Challacombe, M.; Gill, P. M. W.; Johnson, B.; Chen, W.; Wong, M. W.; Gonzalez, C.; Pople, J. A. *Gaussian 03*, revision C.02; Gaussian, Inc.: Wallingford, CT, 2004.
- (28) Frisch, M. J.; Pople, J. A.; Binkley, J. S. *J. Chem. Phys.* **1984**, *80*, 3265.
- (29) Hore, D. K.; Hamamoto, M. Y.; Richmond, G. L. *J. Chem. Phys.* **2004**, *121*, 12589.
- (30) Conboy, J. C.; Messmer, M. C.; Richmond, G. L. *J. Phys. Chem. B* **1997**, *101*, 6724.
- (31) Gragson, D. E.; McCarty, B. M.; Richmond, G. L. *J. Phys. Chem.* **1996**, *100*, 14272.
- (32) Gragson, D. E.; McCarty, B. M.; Richmond, G. L. *J. Am. Chem. Soc.* **1997**, *119*, 6144.
- (33) Gragson, D. E.; Richmond, G. L. *J. Phys. Chem. B* **1998**, *102*, 3847.
- (34) Lu, J. R.; Marrocco, A.; Su, T. J.; Thomas, R. K.; Penfold, J. J. *Colloid Interface Sci.* **1993**, *158*, 303.
- (35) Dominguez, H.; Berkowitz, M. L. *J. Phys. Chem. B* **2000**, *104*, 5302.